N72-27014

NASA TECHNICAL NOTE

NASA TN D-6839

NASA TN D-6839

CASE FILE
COPY

EXPERIMENTAL EVALUATION OF A TF30-P-3 TURBOFAN ENGINE IN AN ALTITUDE FACILITY: AFTERBURNER PERFORMANCE AND ENGINE-AFTERBURNER OPERATING LIMITS

by John E. McAulay and Mahmood Abdelwahab

Lewis Research Center
Cleveland, Ohio 44135

NATIONAL AERONAUTICS AND SPACE ADMINISTRATION • WASHINGTON, D. C. • JULY 1972

EXPERIMENTAL EVALUATION OF A TF30-P-3 TURBOFAN ENGINE IN AN ALTITUDE FACILITY: AFTERBURNER PERFORMANCE AND ENGINE-AFTERBURNER OPERATING LIMITS

by John E. McAulay and Mahmood Abdelwahab

Lewis Research Center

SUMMARY

An investigation was conducted to determine the afterburning steady-state performance and operational limits of a TF30-P-3 turbofan engine. Steady-state performance of the afterburner was obtained over a range of engine-inlet pressures with distortion-free inlet flow. Engine-afterburner altitude operational limits were obtained over a range of engine-inlet distortions during fixed and transient throttle operation. In addition, a limited amount of data was obtained to determine the engine-afterburner limits during time-variant engine-inlet pressure oscillations.

At the Maximum throttle position (full afterburning) the afterburner combustion efficiency and total-pressure-loss ratio were 0.91 and 0.11, respectively, at an engine-inlet Reynolds number index of 0.80. The combustion efficiency decreased to 0.68 at Maximum throttle position and a Reynolds number index of 0.25. During throttle bursts and chops between Military and Maximum throttle position, fan-compressor stalls were encountered. Time histories of pressures in the fan-compressor showed development of rotating stall in the fan hub which quickly propagated and produced complete stall in the high-pressure compressor. The altitude stall limits were substantially reduced as distortion level was increased during either fixed or transient throttle operation. For fixed throttle operation, changing the throttle position from Military to Maximum and closing the compressor bleeds also reduced the altitude stall limits. When time-variant engine-inlet pressure oscillations were imposed, full-face oscillations required the highest amplitude to produce stall. For the other modes of engine-inlet pressure oscillation, the co-rotating distortion caused stall with the lowest amplitude and the lowest instantaneous distortion.

INTRODUCTION

With the progressive development of supersonic aircraft, the demands on the engine and its inlet have increased. These demands or requirements are brought about by the desire for greater maneuverability and for operation at higher flight altitudes and Mach numbers. Greater maneuverability and higher flight numbers impose increasing levels of steady-state and time-variant inlet flow distortions. Higher altitudes produce lower engine-inlet Reynolds numbers. Both the increased level of flow distortions and the decreased Reynolds numbers result in lower fan-compressor stability margins. Furthermore, the lower operating pressures brought about by increased altitude can produce substantial degradation in afterburner combustion efficiency and stability.

In an effort to quantitatively show the effects of engine-inlet pressure level (i.e., altitude) and flow distortions on a modern operational afterburning turbofan engine, a comprehensive program was conducted at NASA Lewis Research Center on the TF30-P-1 and P-3 engines. Results of previously reported nonafterburning tests are given in references 1 to 6. As a part of this overall program, further tests were conducted with the TF30-P-3 engine operating in the afterburning regime. These tests were planned to measure the effect of pressure level, or altitude, on the afterburning steady-state performance and to determine the effect of steady-state and time-variant inlet flow distortions on the engine-afterburner operational limits.

This report presents the results of these tests in the afterburning regime. The afterburner steady-state performance is presented as a function of operating pressure level and fuel-air ratio. Engine afterburner operational limits are shown on coordinates of altitude and distortion level for fixed and transient throttle operation. A limited amount of data is presented at fixed throttle settings to show the effect of several kinds of time-variant engine-inlet flow distortions on engine-afterburner operating limits.

APPARATUS

Engine

The engine used for this investigation was a production TF30-P-3 twin-spool turbofan engine equipped with an afterburner. The engine, shown schematically in figure 1, includes a three-stage axial-flow fan mounted on the same shaft with a six-stage axial-flow low-pressure compressor. This unit is driven by a three-stage low-pressure turbine. A seven-stage, axial-flow compressor driven by a single-stage, air-cooled turbine makes up the high-pressure spool. The overall pressure ratio of the fan-

compressor system is 17, the fan pressure ratio is 2.1, and the bypass ratio is 1.0 at sea-level static Military operating condition.

The compressor is equipped with seventh-stage (low compressor) and 12th-stage (high compressor) bleeds. The seventh-stage bleeds are manually operated and are normally opened at flight Mach numbers above 1.5. The 12th-stage bleeds are normally operated automatically so that they are open at low engine speeds and pressure ratios and closed at the higher speeds and pressure ratios. For this investigation, the 12th-stage bleeds were also manually controlled.

An ejector nozzle having aerodynamically operated blow-in doors and exit leaves is a part of the normal engine-afterburner assembly. For this investigation, the blow-in doors and exit leaves were removed.

Afterburner

The afterburner consists of a diffuser duct, a combustion chamber, a flameholder, and seven fuel spray rings. A cross-sectional schematic of the afterburner showing the location of instrumentation is presented in figure 2. The flameholder and spray ring assembly is shown pictorially in figure 3. The diffuser duct consists of two diffuser sections separated by a splitter cone. Fan air and gas generator gases flow through the outer and inner diffuser ducts, respectively. The combustion section is made up of an outer shell and an inner liner which is perforated at its front and louvered at its aft end. The distance from the forward end of the diffuser section to the aft end of the liner is 257 centimeters. The flameholder is a three-ring V-gutter type. Two of these rings are attached directly to the aft end of the diffuser cone, while the third ring is attached further upstream to the diffuser cone by a rod assembly. The projected blockage of the flameholder is approximately 33 percent of the maximum combustion section area. This blockage is not concentrated at a single axial location.

Scheduling of the afterburner fuel flow and the exhaust nozzle area is accomplished by an integrated afterburner - exhaust nozzle control. This control operates in conjunction with the main engine conditions. The afterburner fuel is introduced into the combustion chamber through the spray rings, which are arranged into five separate zones. Zones 2, 3, and 4 each consist of a fuel line, a manifold, feed tubes, and one spray ring. Fuel fed through these zones mixes with the fan airflow. Zone 5 is similar except that it contains two spray rings. Zone 1 fuel system consists of a fuel flow divider mounted directly on the afterburner fuel control, two fuel lines leading from the flow divider, two fuel manifolds, three feed tubes, and two spray rings. These two paths of zone 1 fuel flow are designated as zone 1 primary and zone 1 secondary. Zone 1 primary is always used when afterburner fuel is flowing. Fuel is introduced

through the zone 1 secondary system only at a main burner pressure level above 124 N/cm^2 abs. Fuel introduced through zones 1 and 5 mixes with the gas generator flow. As afterburner fuel flow is increased, fuel is introduced into gas generator and fan flow successively through zones 1 to 5. Each successive zone fuel flow is additive to the preceding zone flows.

The afterburner nozzle consists of 12 equally spaced segments hinged to the afterburner combustion chamber aft end. These nozzle segments are actuated by six hydraulic cylinders which use fuel as the working fluid. The movement of these segments produces a change in nozzle area.

Distortion Devices

• Engine-inlet spatial total-pressure distortions were produced either by the air jet system or by screens located upstream of the engine inlet. The air jet system was also used to obtain time-variant pressure osciallations at the engine inlet. The screen configurations used during this investigation are shown in figure 4(a). Configurations 1 and 2, which produce the same distortion pattern but are slightly different in magnitude, were designed to reproduce a distortion encountered with the F-111 airplane. The air jet system, which is described in detail in reference 2, is illustrated schematically in figure 4(b). Its primary components are a torus manifold and associated piping, six servo-operated air jet valves of special design (one for each 60° segment) and 54 lines. Each valve supplies high-pressure air to nine lines and in turn to nine jet nozzles located in the engine-inlet duct. The jet nozzles direct the high-pressure air counter to the primary flow from the bellmouth. The high-response servo-operated air jet valves were capable of operating over a range of amplitudes to frequencies of 200 hertz.

Installation

The engine with afterburner and the air jet system are shown installed in the altitude test chamber in figure 5. The air jet system was not installed during the steady-state afterburner performance tests. The installation was a conventional direct-connect type. The engine was mounted on a thrust-measuring stand which consisted of a test bed suspended from facility supports by four flexure plates. The altitude chamber includes a forward bulkhead which separates the inlet plenum from the test chamber. Conditioned air was supplied to the plenum at the desired pressure and temperature and flowed from the plenum through the bellmouth and duct to the engine inlet. When used, the air jet system supplied high-pressure air counter to the primary air approximately

93 centimeters upstream of the engine face (engine-inlet flange). The distortion screens when installed were located 30.5 centimeters upstream of the engine face. For all tests, engine-inlet instrumentation was located 12.5 centimeters upstream of the engine face.

The exhaust gases from the engine were captured by a collector, which extended through the rear bulkhead, to minimize recirculation of these gases into the test chamber. The exhaust pressure is normally controlled by an automatic control valve; but for these tests, this valve was set to its open position. This produced the minimum exhaust pressure for the flow conditions and exhaust equipment used. At an engine-inlet pressure of 5.17 N/cm^2 abs, the exhaust pressure was about 1.9 N/cm^2 abs.

Instrumentation

The station identification and probe locations are shown in figures 1 and 2.

Steady-state instrumentation. - Low pressure levels (0 to 24 N/cm^2) were recorded on a digital, automatic, multiple-pressure recorder. High-pressure levels (above 24 N/cm^2) were measured by means of Scanivalve pressure-measuring devices which used transducers. These devices were capable of measuring 48 pressures with each transducer during one cycle of data recording. The operation of the Scanivalves and the recording of their output was accomplished through use of the central automatic digital data encoder and the automatic voltage digitizer. Chromel-Alumel thermocouples were used to measure temperatures, and the outputs were recorded by means of the automatic voltage digitizer. These recording systems are described in detail in reference 7. A water-cooled load cell was used to measure thrust.

High-response transient instrumentation. - High-response transient instrumentation and recording systems were used to measure instantaneous distortion levels and rapid pressure variations, particularly those associated with stall. In addition, this type of instrumentation system made it possible to properly define the sequence of events in the engine when these events occurred within milliseconds of each other. The number and location of the transient probes are shown in figure 1. This instrumentation was designed to have a frequency response to at least 300 hertz with a maximum amplitude error no greater than ±5 percent. The design, cooling, method of calibration, and recording of this instrumentation are described in reference 3.

PROCEDURE

For all tests the exhaust pressure was maintained at a value low enough to ensure choked flow at the exhaust nozzle exit.

Steady-State Performance

The steady-state performance of the afterburner was obtained with uniform engine-inlet flow (i.e., air jet system or distortion screens not installed in engine-inlet duct). The seventh- and 12th-stage compressor bleeds were closed. The engine-inlet conditions were stabilized at engine-inlet total pressures corresponding to Reynolds number indices of 0.80, 0.50, 0.35, and 0.25 and an engine-inlet temperature of near 16° C. At each engine-inlet Reynolds number index, data were taken with the throttle set at Military (i.e., the highest nonafterburning throttle position) and at approximately 10 different afterburning throttle settings between the lowest afterburning throttle setting and Maximum (i.e., the highest afterburning throttle position).

Engine Afterburner Operational Limits

The engine afterburner operational limits were obtained for three different operational modes: transient throttle at fixed levels of engine-inlet pressure and distortion, fixed throttle while slowly (quasi-steady-state) changing engine-inlet pressure and/or distortion, and fixed throttle while imposing time-variant engine-inlet pressure oscillations. The methods and conditions at which these data were obtained are summarized in the following discussion and in table I.

Transient throttle. - These tests were essentially the same whether the air jet system or screens were used to produce the distortion. The engine-inlet pressure and distortion were set at the desired levels with the engine throttle set at Military. (When screens were used, the distortion level produced by the particular screen configuration used was accepted.) Steady-state data were taken and the transient data systems were activated. The engine throttle was then rapidly moved from Military to Maximum in about 1 second (throttle burst). If stall or blowout did not occur, the engine and afterburner were allowed to stabilize for about 10 seconds and then the throttle was rapidly moved to Military (throttle chop). Depending on whether an engine-afterburner limit was reached (i.e., stall or blowout), the engine-inlet pressure was either raised or lowered and the preceding procedure repeated. This was continued until the engine-afterburner limit was narrowly bracketed.

Fixed throttle. - The engine throttle and compressor bleeds were set at their desired positions with uniform flow at the engine inlet. When an inlet distortion was desired, the air jet system was used to slowly impose a predetermined distortion level. Steady-state data were then taken and the transient data systems activated. The engine-inlet pressure was then gradually lowered until an engine-afterburner limit was reached.

Time-variant pressure oscillation tests were also conducted at fixed throttle. After the engine throttle and the compressor bleeds were set, steady-state data were taken and the transient data systems were activated. An analog computer was used to control the air jet valves so that the engine-inlet pressure phasing and amplitude were programmed. The inlet pressure amplitude was gradually increased until an engine-afterburner limit or a valve amplitude limit was reached. For the tests conducted and reported herein the input frequency of the pressure oscillations was 20 hertz. This frequency was selected because the air jet system was capable of producing high engine-inlet pressure amplitudes to frequencies near 20 hertz.

RESULTS AND DISCUSSION

Steady-State Performance

The steady-state performance of the afterburner is presented in figure 6 to 8 for a range of engine-afterburner pressure levels and afterburner fuel-air ratios. For all data shown, the average afterburner-inlet velocity (station 8) and temperature varied from 91 to 96 meters per second and 111° to 118° C in the fan airstream and from 207 to 222 meters per second and 571° to 625° C in the gas generator stream. The temperature range for the fan and gas generator flows is associated with engine-inlet Reynolds number index, with the higher values corresponding to the lower indices. The methods of calculation for the various parameters are given in appendix A. Symbols are defined in appendix B.

Combustion efficiency. - The variation of afterburner combustion efficiency with fuel-air ratio for engine-inlet Reynolds number indices of 0.80, 0.50, 0.35, and 0.25 is presented in figure 6. Zones 1 and 5, which are the zones where fuel is injected into the primary or core flow, have significantly greater fuel-air ratio ranges than zones 2 to 4. Fuel introduced through these latter zones is directed into the bypass or fan flow.

The change in combustion efficiency with fuel-air ratio is generally larger within the zone 1 range of fuel-air ratios than in any of the other four zones. If the very low fuel-air ratios of zone 1 at indices of 0.35 and 0.25 are excluded, there are only small variations in efficiency with fuel-air ratio at a given Reynolds number index.

At all fuel-air ratios there is a significant effect of pressure level on combustion efficiency. At full afterburning in zone 5 (i.e., Maximum throttle position) the efficiency declined from 0.91 to 0.68 as engine-inlet Reynolds number index was lowered from 0.80 to 0.25. For all zones, a decrease in index from 0.80 to 0.25 produced a

reduction in efficiency of between 0.14 and 0.34. This decrease in index corresponds to an afterburner-inlet pressure decline from 1.62 atmospheres to 0.51 atmosphere. Most of the loss in efficiency occurred as the Reynolds number index was reduced below a value of 0.50.

Pressure-loss and temperature-rise ratios. - The afterburner total-temperature-rise and total-pressure-loss ratios are presented in figure 7 as a function of fuel-air ratio for engine-inlet Reynolds number indices of 0.80, 0.50, 0.35, and 0.25. These data show that the afterburner temperature-rise ratio (fig. 7(a)) increases with fuel-air ratio at a given pressure level (i.e., Reynolds number index) and with pressure level at a given fuel-air ratio. The increased temperature ratios produce higher afterburner momentum pressure losses and, consequently, higher total-pressure losses, as shown in figure 7(b). At the full-afterburner condition, the pressure-loss ratio was about 0.11 at an engine-inlet Reynolds number index of 0.80.

Specific fuel consumption and augmented thrust ratios. - The afterburner specific fuel consumption and augmented thrust ratios are presented in figure 8 for a range of fuel-air ratios at engine-inlet Reynolds number indices of 0.80, 0.50, 0.35, and 0.25. (These data, as previously mentioned, were obtained with the blow-in doors and exit leaves removed.) For both ordinates, the ratios are determined by using the values at Military throttle position as a base level. The results of these data reflect the trends shown in figure 6. At the Maximum throttle position and at an index of 0.80, the specific fuel consumption ratio was 2.06 and the augmented thrust ratio was 1.56.

Operational Limits

Engine-afterburner operational limits are presented in figures 9 to 17. Operational limits during this investigation were manifested by fan-compressor stall or afterburner blowout.

Transient throttle limits. - Typical time histories of a number of engine-afterburner parameters during a stall-free throttle burst and chop between Military and Maximum throttle positions are shown in figure 9. The afterburner ignition, as evidenced by the first rapid increase in engine and afterburner pressures, occurred about 1.6 seconds after initiation of the throttle burst. Subsequent ignition of each of the afterburner zones is shown by a rise in pressures and a stepwise increase in exhaust nozzle area. The particularly large rise in afterburner fuel flow between 2.4 and 2.9 seconds is related to the main afterburner fuel pump being activated. At the lower afterburner fuel flows, the afterburner hydraulic fuel pump supplied fuel to the afterburner. The throttle chop occurred much more rapidly than the throttle burst (i.e., in less than 2 sec compared with about $8\frac{1}{2}$ sec). During the throttle chop, the fuel flow and nozzle

area were not staged through each afterburner zone, as was observed during the throttle burst.

Time histories of engine-afterburner pressures acquired from a higher-response data system than that used for the data presented in figure 9 are shown in figure 10. The data of figure 10 display the results of a number of engine pressures during a throttle burst (fig. 10(a)) and a throttle chop (fig. 10(b)) during which stall occurred. For both the burst and chop the stall sequences were quite similar, so that the following discussion will be directed specifically toward the throttle burst data. The total time for which data are shown is 150 milliseconds (fig. 10(a)). During this time, afterburner ignition, stall initiation, and a complete flow breakdown with accompanying hammershock occurred. (The comparable time of events in figure 9 was between about 1.55 and 1.70 sec.) The stall shown by the data of figure 10(a) occurred following afterburner ignition and its associated pressure rise.

The first significant event exhibited in figure 10(a) is afterburner ignition, which is denoted by a rise in the exhaust nozzle inlet pressure about 1650 milliseconds after the start of the throttle movement. This event is quickly followed by a rise in the level of the fan exit pressures. Soon after ignition and coincident with the rising fan exit pressure levels, there is an increase in the activity or amplitude of these pressures. High-response data taken with the engine during steady-state nonafterburning and afterburning conditions exhibited similar trends in fan exit pressure amplitude, indicating that the higher amplitudes are due to the afterburning process. Of the pressures shown in figure 10(a), the fan hub exit pressure near the flow splitter ($P_{t,2.3\text{-}88^{o}\text{-}1}$) showed the largest increase in amplitude as the afterburner regime was entered.

At 1745 milliseconds from the initiation of the throttle burst there is a substantial pressure drop followed by recovery of the fan exit pressure nearest the flow splitter ($P_{t,2.3\text{-}88^{o}\text{-}1}$). This is followed 7 milliseconds later by a pressure drop and recovery at several axial locations ($P_{t,2.3\text{-}269^{o}\text{-}2}$, $P_{t,3\text{-}261\text{-}2}$, and $P_{t,3.12\text{-}269^{o}\text{-}1}$) in the gas generator flow on the other side of the engine (i.e., about 180° circumferentially from $P_{t,2.3\text{-}88^{o}\text{-}1}$). The 7-millisecond time interval is compatible with past experience, which has demonstrated that rotating stall zones move at about one-half rotor speed. Three to 4 milliseconds later, the high-pressure compressor stalls completely, as indicated by the rapid decline of its mid-stage $P_{t,3.12}$ and exit $P_{t,4}$ pressures and the subsequent hammershock at fan and compressor axial locations upstream of the high-pressure compressor. Although these time histories show the apparent development of a rotating stall in the fan hub which quickly propagated and produced complete stall in the high-pressure compressor, it should be kept in mind that a more detailed analysis of the flow is required before the exact mechanism can be determined. A similar chain of events leading to complete stall during a throttle chop is illustrated by the data of figure 10(b).

Another perspective of the events exhibited by the data of figure 10 is shown in figure 11. This figure shows the movement of the fan-compressor operating points as defined by corrected speed and pressure ratio during a stall-free throttle burst and chop between Military and Maximum throttle positions. Also shown in this figure are stall limits as a function of corrected speed. These stall limits are based on results obtained from the engine manufacturer's unpublished component rig data and Arnold Engineering Development Center (AEDC) data (ref. 8). Because of differences in testing methods, instrumentation, and test hardware, the stall limits are not necessarily compatible with the transient variation of fan-compressor operating points. However, these limits are useful in providing a relative picture of the stall margin available for the various fan-compressor components. The data of figure 11 show that for the stall-free throttle transient data presented, the fan hub is the component which would probably initiate stall. This conclusion agrees with the data presented in figure 10.

The results displayed in figures 9 to 11 give some insight into what is happening in the fan-compressor system during typical throttle bursts and chops between the Military and Maximum throttle positions. The overall results of a series of these throttle bursts and chops over a range of altitudes and 180° steady-state distortions is shown in figure 12 for a simulated flight Mach number of 1.4 (see PROCEDURE for a description of how the data were obtained). The inlet air temperature ($\sim 34^{\circ}$ C) established the simulated Mach number for altitudes above the tropopause. The altitude was defined by the distortion-free inlet pressure adjusted by an appropriate inlet pressure recovery (i.e., 0.978 for Mach 1.4). The distortion level, which was produced by using the air jet system, was a function of the average and the minimum engine-inlet pressures and is presented in the form of differential pressure divided by average pressure. All the engine afterburner limits displayed were obtained with the seventh- and 12th-stage compressor bleeds closed and were a result of fan-compressor stall. For the throttle burst mode of operation the altitude limit was about 18 900 meters with no inlet distortion. At a distortion level of 5 percent the altitude throttle burst limit was reduced to 12 800 meters. During throttle chops the altitude limits were substantially lower than for throttle bursts. At distortion levels of zero and 5 percent the throttle chop altitude limits were 15 850 and 12 040 meters, respectively.

Throttle bursts and chops were also tried at a simulated flight Mach number of 2.5. The data are presented in figure 13 on coordinates of altitude and engine-inlet distortion (i.e., the same as for fig. 12). For this simulated Mach number, the inlet pressure recovery was assumed to be 0.871, and the inlet distortions were produced by screens. The seventh-stage compressor bleeds were open and the 12-stage bleeds were closed. The only stalls encountered occurred with screen configuration 3 and the engine control trimmed above its normal level (i.e., higher than normal engine speed for Military throttle position). Even in this instance, stall was obtained only above an altitude of

18 600 meters with a distortion level of about 5.4 percent and the 12th-stage bleeds manually closed. When the 12th-stage bleeds were allowed to operate in their automatic mode, they would open above an altitude of about 17 070 meters, thus preventing stall. No instances occurred, such as had at Mach 1.4, where a successful throttle burst was made followed by an unsuccessful (i.e., stall) throttle chop.

Fixed throttle limits. - For these tests, the engine-inlet pressure was slowly decreased at several fixed throttle positions and inlet distortion levels. The change in inlet pressure, which is related to altitude for a given Mach number, was slow enough so that engine conditions were quasi steady-state. Typical time histories of several engine-afterburner pressures at fixed afterburner throttle position are shown in figure 14 at the time an operational limit was reached. Two test points are presented - one which resulted in stall, the other in afterburner blowout. Stall is a result of the effect of engine-inlet Reynolds number on the engine operating and stall lines. Blowout is a result of reaching a pressure level which is unable to support combustion.

The results of a series of fixed throttle tests similar to those presented in figure 14 are summarized in figure 15 on coordinates of altitude and distortion for a simulated flight Mach number of 1.4. Data are shown for several combinations of seventh- and 12th-stage bleed positions and three throttle positions - Military, partial afterburning, and Maximum (i.e., full afterburning). During afterburning operation with minimum facility inlet distortion, both afterburner blowout and fan-compressor stall were limiting at an altitude of about 19 800 meters. The data also show that the altitude stall limits were substantially reduced (1) as distortion level was increased (2) as throttle position was changed from Military to Maximum, and (3) as the compressor bleeds were closed.

The more important results of figures 12 and 15 were combined and are presented in figure 16 for the same coordinate system, altitude and distortion. As might be expected, the transient throttle limits occur at lower altitudes and distortion levels than the fixed throttle limits.

Time-variant distortion at fixed throttle. - The effect of engine-inlet pressure oscillations at fixed throttle position on engine-afterburner operation is described by the bar chart presented in figure 17. These oscillations were imposed at only one frequency for these tests, 20 hertz. (A detailed discussion on the characteristics of a nonafterburning turbofan engine during time-variant engine-inlet pressures is given in ref. 5.) The length of the bars represents the imposed normalized amplitude of the engine-inlet pressure $(P_{t,2,max} - P_{t,2,min})/P_{t,2,av}$ which produced stall or was limited by the air jet system. To the right of each bar a maximum instantaneous distortion $(P_{t,2,av} - P_{t,2,min})/P_{t,2,av}$ is given. For the 180° out-of-phase, the contra-rotating, and the co-rotating pressure oscillations, the instantaneous distortion value is simply one-half of the normalized amplitude. For the full-face pressure oscillations, the distortion is essentially the minimum facility distortion (i.e., about 1.5 percent) and is consistent

with experimental levels previously determined (ref. 5).

The data of figure 17 show that the full-face inlet pressure oscillations required normalized amplitudes of two to three times that required for the other types of oscilations in order to produce stall. Of the other three modes of inlet pressure oscillation, the co-rotating distortion caused stall with the lowest amplitude and the lowest instantaneous distortion. For all the types of inlet pressure oscillation investigated, the effect of increased throttle position and closing of the seventh-stage bleeds was to reduce the amplitude and/or distortion required to produce stall.

SUMMARY OF RESULTS

An investigation was conducted to determine the performance and operational characteristics of a TF30-P-3 turbofan engine in its afterburning regime. The principal results of this investigation were as follows:

1. At the Maximum throttle position (full afterburning) the afterburner combustion efficiency declined from 0.91 to 0.68 as the engine-inlet Reynolds number index was lowered from 0.80 to 0.25. If the very low fuel-air ratios of zone 1 at indices of 0.35 and 0.25 are excluded, there are only small variations in efficiency with fuel-air ratio at a given Reynolds number index.

2. At the Maximum throttle position at a Reynolds number index of 0.80, the afterburner total-pressure-loss ratio was about 0.11.

3. During throttle bursts and chops between Military and Maximum throttle position, fan-compressor stalls were encountered. Time histories of pressures in the fan-compressor show the development of rotating stall in the fan hub which quickly propagated and produced complete stall in the high-pressure compressor.

4. The altitude stall limits were substantially reduced as distortion level was increased during either fixed or transient throttle operation. For fixed throttle operation, changing the throttle position from Military to Maximum and closing the compressor bleeds also reduced the altitude stall limits.

5. When time-variant engine-inlet pressure oscillations were imposed, full-face oscillations required the highest amplitude to produce stall. For the other modes of engine-inlet pressure oscillation, the co-rotating distortion caused stall with the lowest amplitude and the lowest instantaneous distortion.

Lewis Research Center,
National Aeronautics and Space Administration,
Cleveland, Ohio, April 7, 1972,
764-74.

APPENDIX A

METHOD OF CALCULATION

Airflow

Primary airflow at the engine inlet was calculated from an enthalpy average of

$$W_{a,1} = (PAM)_1 \sqrt{\left(\frac{\gamma}{T_t}\right)_1 \left(\frac{g}{R_g}\right) \left(\frac{P_t}{P}\right)_1^{[(\gamma-1)/\gamma]_1}}$$

Gas Flow

The afterburner gas flow is the sum of the measured air and fuel flow.

$$W_{g,9} = W_{a,1} + W_{fu,t}$$

Afterburner Fuel-Air Ratio

The afterburner fuel-air ratio was defined as the ratio of the afterburner fuel flow to the unburned air entering the afterburner. Engine combustion efficiency was assumed to be 100 percent.

$$(f/a)_{A/B} = \frac{W_{fu,t} - W_{fu,e}}{W_{a,1} - \frac{W_{fu,e}}{0.06746}}$$

where 0.06746 is the stoichiometric fuel-air ratio of the fuel used.

Afterburner-Inlet Total Pressure

The afterburner-inlet total pressure, station 8, was calculated from the following equation:

$$P_{t,8} = \frac{A_{7f}}{A_{7f} + A_{7g}} P_{t,7f} + \frac{A_{7g}}{A_{7f} + A_{7g}} P_{t,7g}$$

Afterburner Inlet Total Temperature

The afterburner inlet total temperature was calculated from an enthalpy average of the fan and core streams at the afterburner inlet.

Total Pressure at Exhaust Nozzle Inlet

The total pressure at the exhaust nozzle inlet (station 9) was calculated by assuming a constant momentum between stations 8 and 9 (ignoring body force due to area change).

$$P_{t,9} = P_9 \left[1 + \left(\frac{\gamma - 1}{2\gamma} \right)_9 \left\{ \left(1 + \gamma M^2 \right)_8 \frac{(PA)_8}{(PA)_9} - 1 \right\} \right]^{\left(\frac{\gamma}{\gamma - 1} \right)_9}$$

Afterburner Combustion Temperature

The afterburner combustion temperature was calculated by using the measured gross thrust and the gas weight flow. The exhaust nozzle was assumed to be choked.

$$T_{t,j} = \left[\frac{F_G}{(C_{v,e})(W_{g,9}) \sqrt{\frac{\left(R_g \gamma \right)_9}{g}} \left(\frac{T}{T_t} \right)_j^* \left\{ 1 + \frac{1}{\gamma_9} \left[1 - \frac{P_{10}}{P_{t,9}} \left(\frac{P_t}{P} \right)_j^* \right] \right\}} \right]^2$$

where the asterisk denotes conditions at Mach 1.0. The effective velocity coefficient $C_{v,e}$ was obtained from nonafterburner data (assuming $T_{t,j} = T_{t,8}$).

Afterburner Combustion Efficiency

The combustion efficiency is defined as the ratio of the actual temperature rise to the ideal temperature rise.

$$\eta_{A/B} = \frac{T_{t,j} - T_{t,8}}{T_{t,j,id} - T_{t,8}}$$

where $T_{t,j,id}$ was calculated from an enthalpy balance based on an adiabatic combustion process (dissociation effects included).

Engine Net and Gross Thrust

The engine afterburner net thrust is defined as

$$F_n = F_G - F_{ram}$$

where

F_n net thrust

F_G gross thrust

F_{ram} ram thrust, $(W/gV)_\infty$

The gross thrust is defined as

$$F_G = F_m + F_p + F_l$$

where

F_m load-cell measurement

F_p total momentum at station 1

F_l labyrinth seal A ΔP

Calibration factor for the labyrinth seal A ΔP was obtained from previous calibrations.

Specific Fuel Consumption

The combined engine and afterburner specific fuel consumption was defined as

$$SFC = \frac{W_{fu,t}}{F_n}$$

Augmented Thrust Ratio

The augmented thrust ratio $F_G/F_{G,mil}$ was defined as the augmented gross thrust to the thrust at Military conditions (maximum nonafterburning throttle position).

Specific Fuel Consumption Ratio

The specific fuel consumption ratio SFC/SFC_{mil} was defined as the augmented specific fuel consumption to the specific fuel consumption at Military conditions (maximum nonafterburning throttle position).

APPENDIX B

SYMBOLS

A	flow area, m^2
$C_{v,e}$	effective velocity coefficient
F	thrust, kgf
f/a	fuel-air ratio
g	acceleration due to gravity, 9.8066 m/sec^2
M	Mach number
N_1	low rotor speed, rpm
N_2	high rotor speed, rpm
P	static pressure, N/cm^2
P_t	total pressure, N/cm^2
ReI	Reynolds number index, $\delta_{2.0}/(\mu_{2.0}/\mu_{sl})\sqrt{\theta_{2.0}}$
R_g	gas constant, J/(kg)(K)
SFC	specific fuel consumption, (kgf)(hr)/(kgf thrust)
T	static temperature, ^oC
T_t	total temperature, ^oC
V	velocity, m/sec
W	weight flow rate, kgf/sec
γ	ratio of specific heats
δ	ratio of total pressure to standard sea-level static pressure
η	combustion efficiency
θ	ratio of total temperature to standard sea-level static temperature
μ	absolute viscosity, $N\text{-}sec/m^2$
∞	free-stream conditions

Subscripts:

A/B	afterburner
a	air
av	average

e	engine
f	fan duct
fu	fuel
G	gross
g	gas
id	ideal
j	within jet at exhaust nozzle exit plane
mil	Military
min	minimum
max	maximum
sl	sea level
t	total conditions
0	bellmouth inlet
1	airflow metering station
2	fan or engine inlet
2.3	fan hub exit
2.3f	fan tip exit
2.6	low-pressure-compressor mid-stage (sixth-stage stator)
3	low-pressure-compressor exit, high-pressure-compressor inlet
3.12	high-pressure-compressor mid-stage (twelfth-stage stator)
4	high-pressure-compressor exit
7g	turbine exit
7f	fan duct exit
8	averaged flow at afterburner inlet
9	exhaust nozzle inlet
10	external environment at exhaust nozzle exit plane

REFERENCES

1. Braithwaite, Willis M.; and Volmar, William R.: Performance and Stall Limits of a YTR30-P-1 Turbofan Engine with Uniform Inlet Flow. NASA TM X-1803, 1969.

2. Meyer, Carl L.; McAulay, John E.; and Biesiadny, Thomas J.: Technique for Inducing Controlled Steady-State and Dynamic Inlet Pressure Disturbances for Jet Engine Tests. NASA TM X-1946, 1970.

3. Braithwaite, Willis M.; Dicus, John H.; and Moss, John E., Jr.: Evaluation with a Turbofan Engine of Air Jets as a Steady-State Inlet Flow Distortion Device. NASA TM X-1955, 1970.

4. Werner, Roger A.; Abdelwahab, Mahmood; and Braithwaite, Willis M.: Performance and Stall Limits of an Afterburner-Equipped Turbofan Engine with and without Inlet Flow Distortion. NASA TM X-1947, 1970.

5. McAulay, John E.: Effect of Dynamic Variations in Engine-Inlet Pressure on the Compressor System of a Twin-Spool Turbofan Engine. NASA TM X-2081, 1970.

6. Wenzel, Leon M.: Experimental Investigation of the Effects of Pulse Pressure Distortions Imposed on the Inlet of a Turbofan Engine. NASA TM X-1928, 1969.

7. Staff of Lewis Laboratory: Central Automatic Data Processing System. NACA TN 4212, 1958.

8. Palmer, J. D.; Parker, J. R.; and Schwall, J. R.: Effect of Steady Inlet Distortion on the Stability and Performance Characteristics of an Augmented Turbofan Engine. Rep. ARO-ETF-TR-70-322, ARO, Inc. AEDC-TR-71-50, AD-882311L, Apr. 1971.

TABLE I. - SUMMARY OF OPERATIONAL LIMITS TESTS[a]

Engine throttle		Seventh-stage bleeds	Twelfth-stage bleeds	Engine-inlet environment	Simulated flight Mach number	Engine-inlet temperature, ^{o}C
Operation	Position (b)					
Transient (bursts and chops)	Military to Maximum; Maximum to Military	Closed	Closed	Steady state (range of inlet distortions including distortion-free flow)[c]. Range of altitudes.	1.4	~34
		Open	Closed	Several levels of circumferential distortion (screens). Range of altitudes.	2.5	~216
Fixed	Military A/B 3 Maximum ↓	Closed ↓ Open Open	Closed Closed Closed Open Closed Open	Slow (quasi steady-state) decrease in engine-inlet pressure with distortion-free inlet flow[c]. Range of altitudes.	1.4 ↓	~34 ↓
	Military A/B 3 Maximum Maximum	Closed Closed Closed Open	Closed ↓	Slow (quasi steady-state) decrease in engine-inlet pressure with several levels of 180° circumferential distortion. Range of altitudes.	1.4 ↓	~34 ↓
	Military Maximum Maximum	Closed Closed Open	Closed Closed Closed	Full-face cyclic; 180°-out-of-phase cyclic distortion; co- and contra-rotating distortion. Altitude, 15 250 m.	1.4 1.4 1.4	~34 ~34 ~34

[a]All distortions were obtained by using the air jet system at Mach 1.4 and screens at Mach 2.5.

[b]Military - highest nonafterburning throttle position. A/B 3 - throttle position for afterburning in zone 3. Maximum - highest afterburning throttle position (zone 5).

[c]Distortion-free inlet flow is minimum facility distortion and is about 1.5 percent.

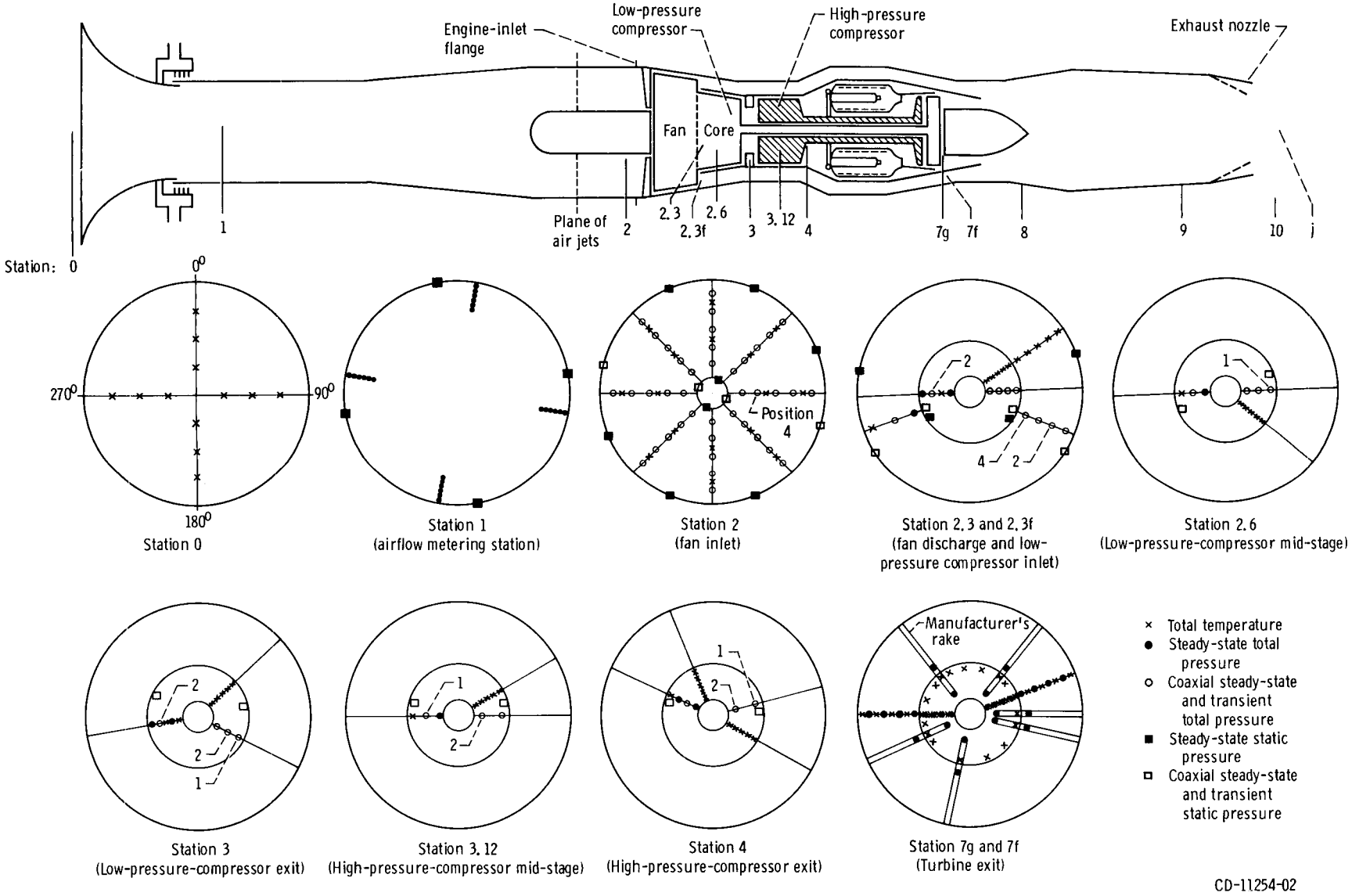

Figure 1. - Instrumentation layout for TF30-P-3 turbofan engine. (Instrumentation stations viewed looking upstream.)

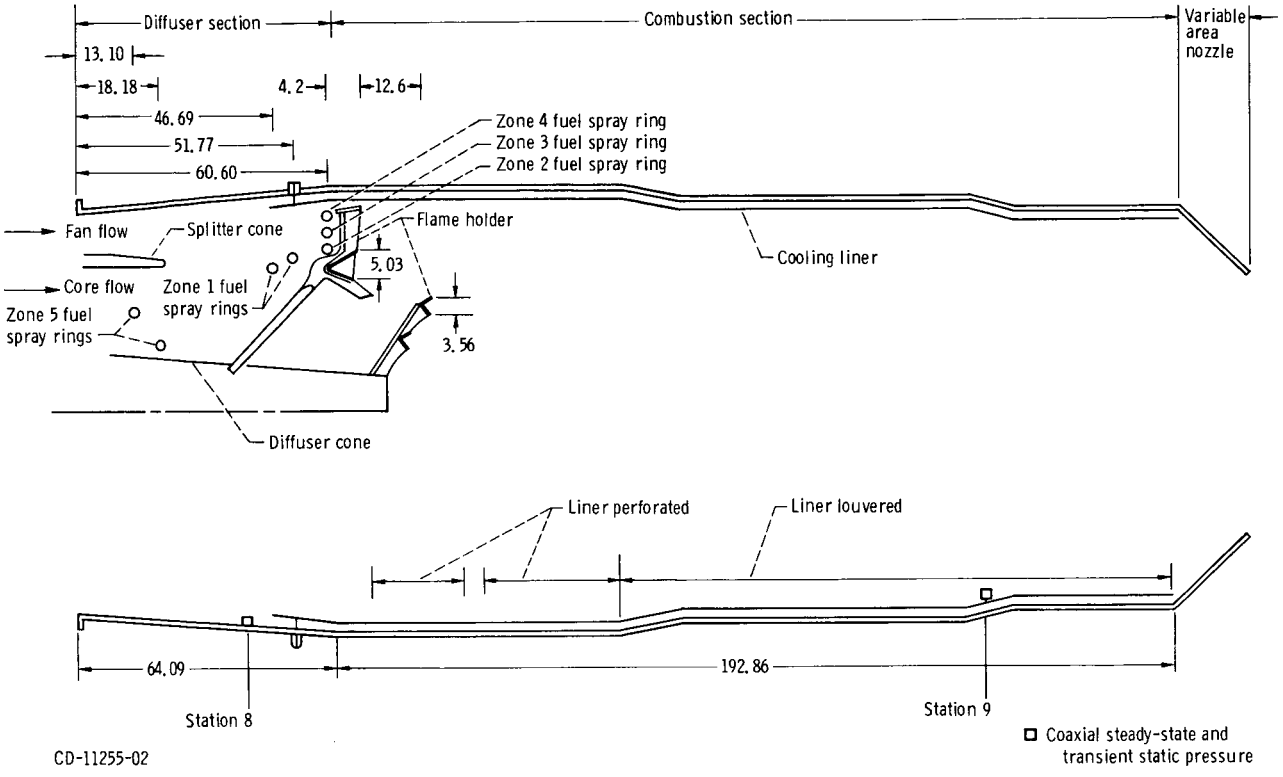

Figure 2. - Cross-sectional schematic of afterburner with instrumentation locations. (All dimensions in centimeters.)

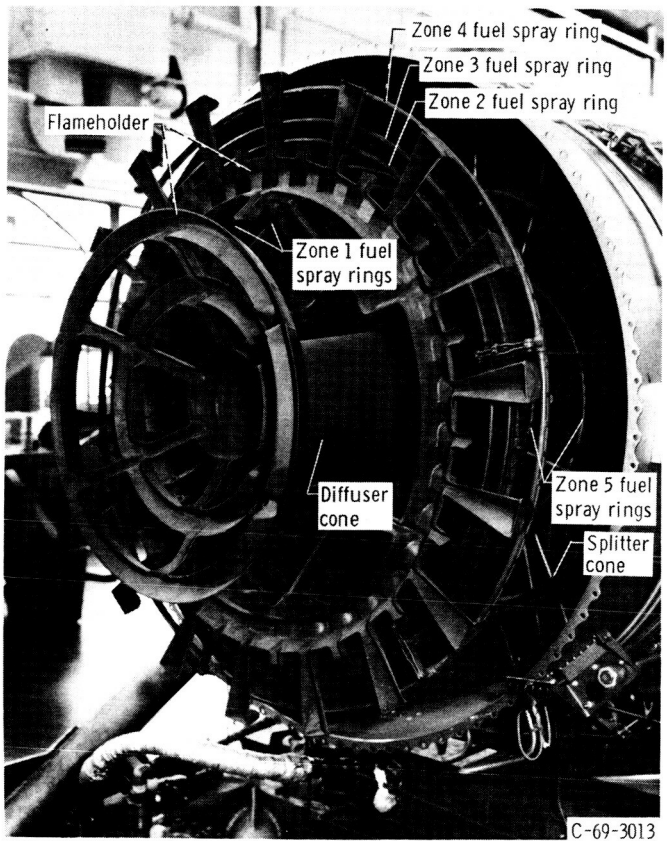

Figure 3. - Afterburner flameholder and spray rings assembly. View looking upstream.

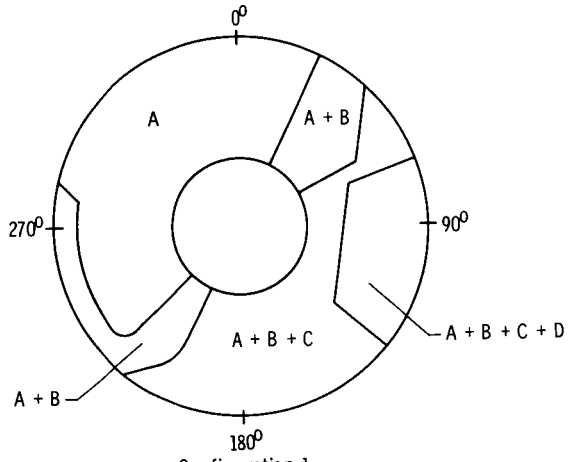

Configuration 1

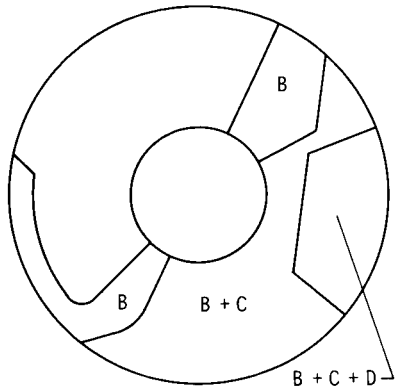

Configuration 2

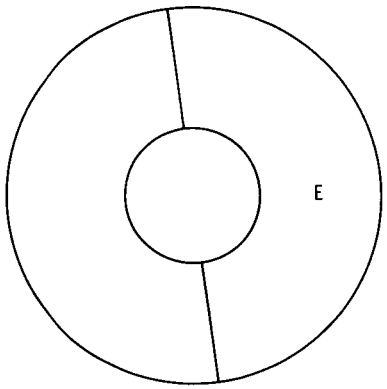

Configuration 3

Screen	Width of opening, mm	Wire diameter, mm	Percent blockage	Circumferential extent, deg
A	11.10	1.60	23.6	360
B	4.75	1.60	44.0	28 to 283
C	4.75	1.60	44.0	43 to 218
D	4.75	1.60	44.0	68 to 128
E	1.764	1.83	59.0	8 to 188

The supporting structure (which extended 360° circumferentially) is made up of 12 struts, equally spaced circumferentially, and a backup screen consisting of 3.048-mm-diameter wires spaced 50.8 mm apart.

(a) Screen configurations. View looking upstream.

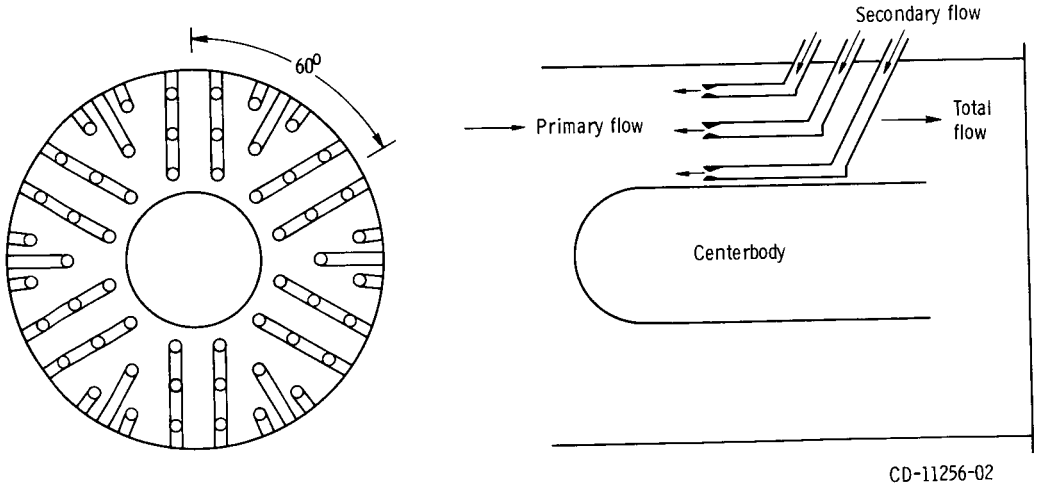

(b) Schematic drawing of jet array.

Figure 4. - Schematic of distortion devices.

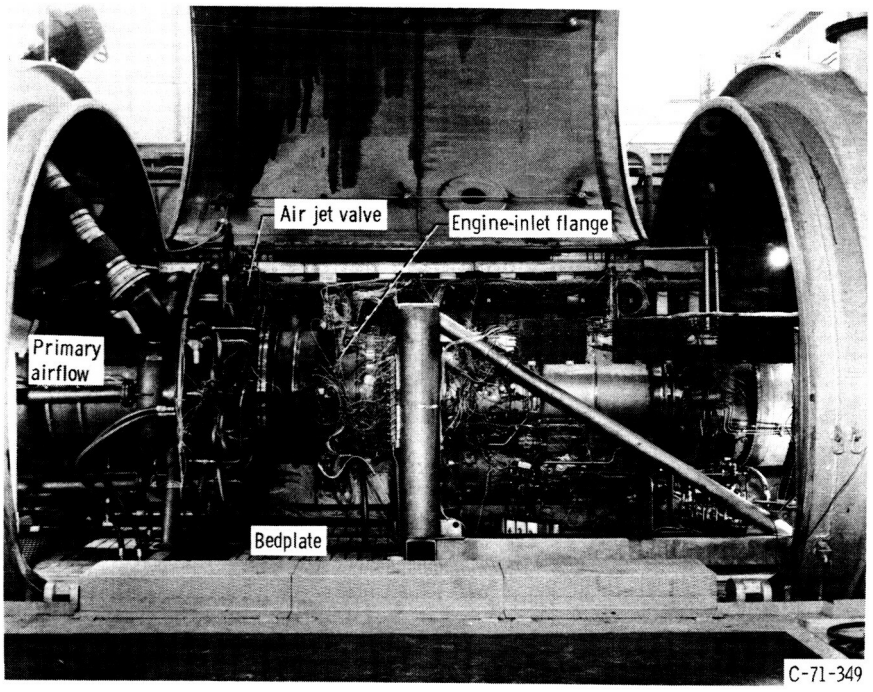

Figure 5. - Afterburning turbofan with air jet system installed in altitude test chamber.

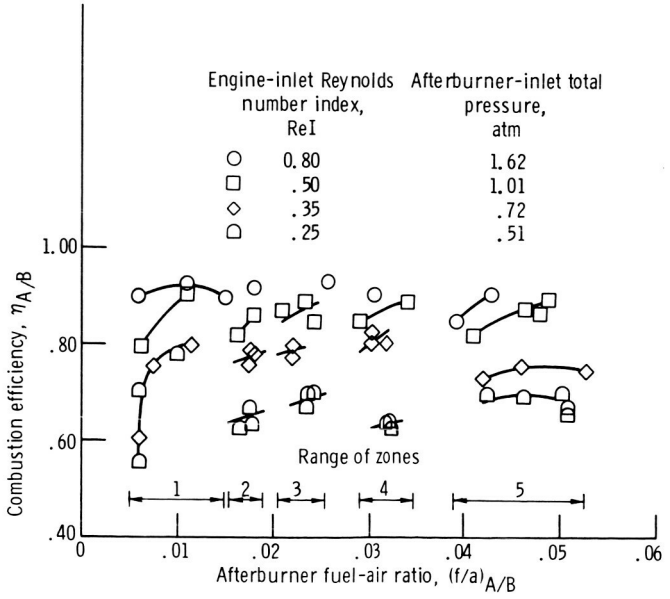

Figure 6. - Effect of afterburner pressure level and fuel-air ratio on afterburner combustion efficiency with steady-state distortion-free engine-inlet flow. Engine-inlet temperature, 16^0 C.

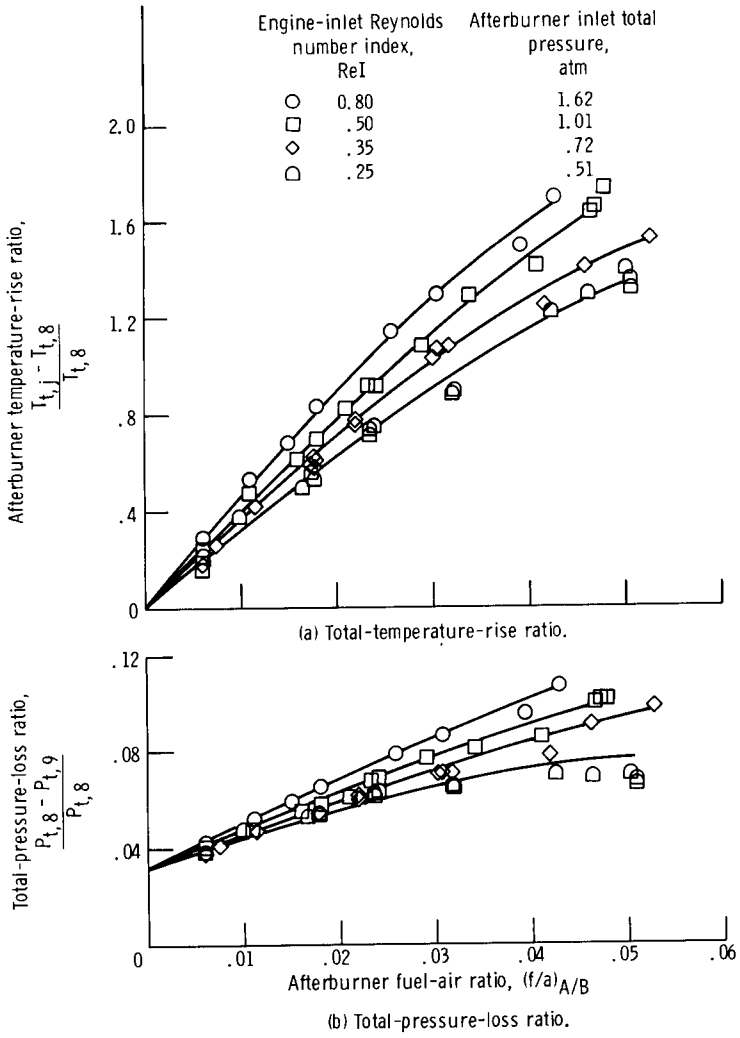

(a) Total-temperature-rise ratio.

(b) Total-pressure-loss ratio.

Figure 7. - Effect of afterburner pressure level and fuel-air ratio on afterburner pressure loss and temperature rise with steady-state distortion-free engine-inlet flow. Engine-inlet temperature, 16^0 C.

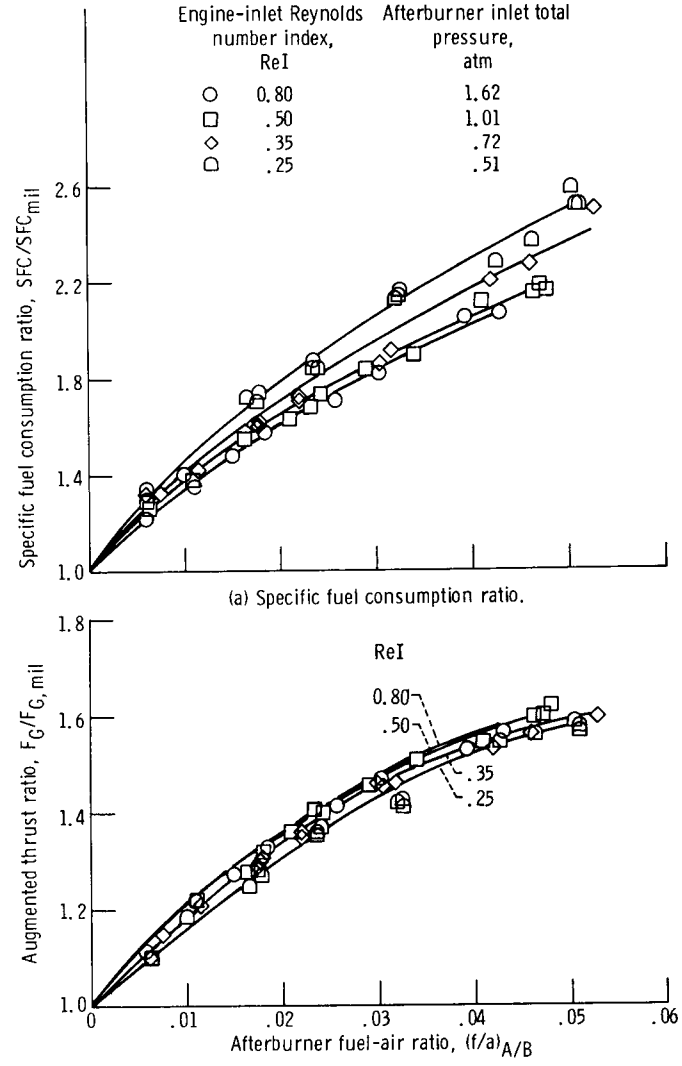

(a) Specific fuel consumption ratio.

(b) Augmented thrust ratio.

Figure 8. - Effect of afterburner pressure level and fuel-air ratio on specific fuel consumption ratio and augmented thrust ratio with steady-state distortion-free engine-inlet flow. Engine-inlet temperature, 16^0 C.

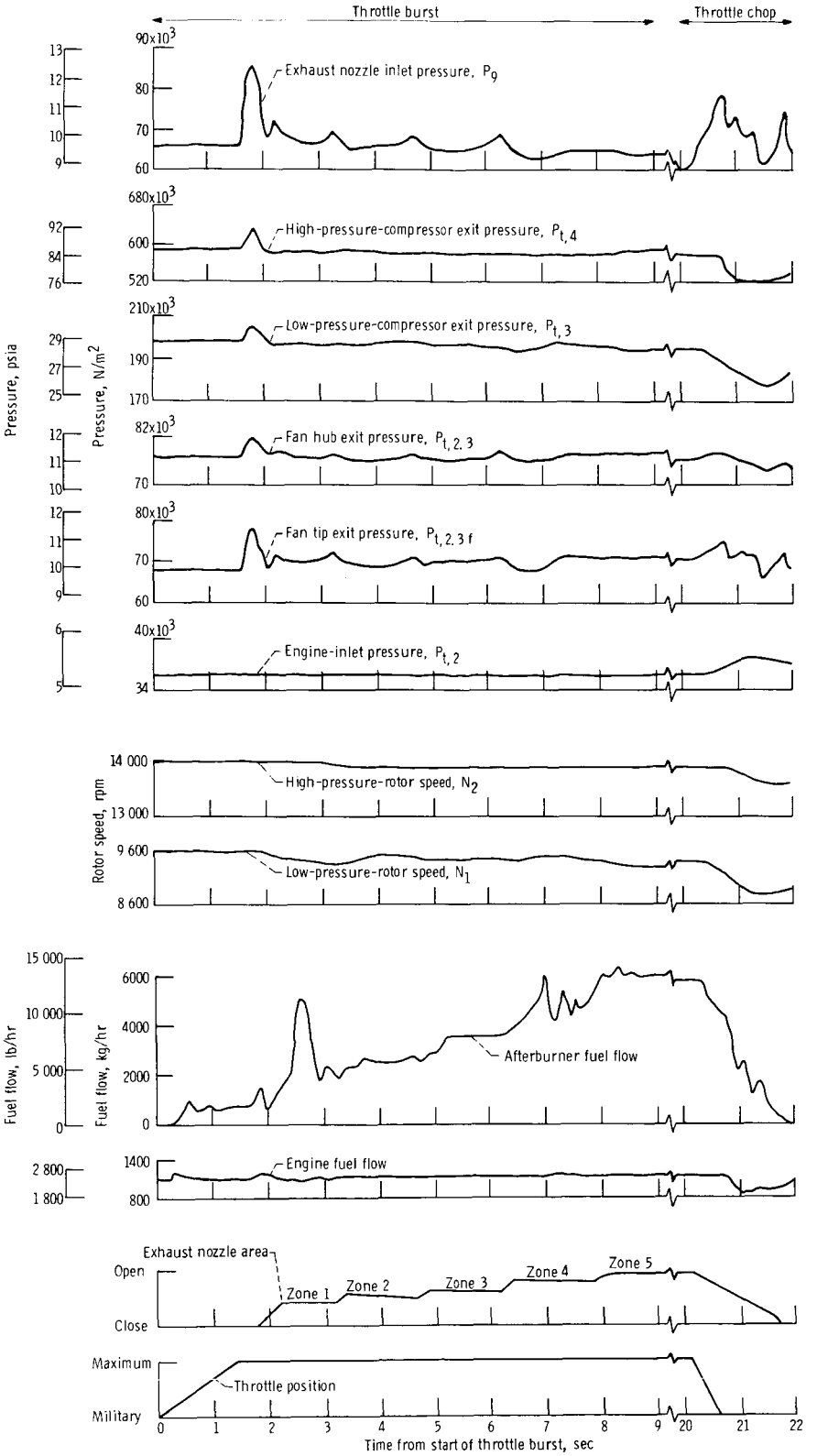

Figure 9. - Typical stall-free time history of engine-afterburning parameters during throttle burst and chop between military and maximum throttle positions with distortion-free engine-inlet flow.

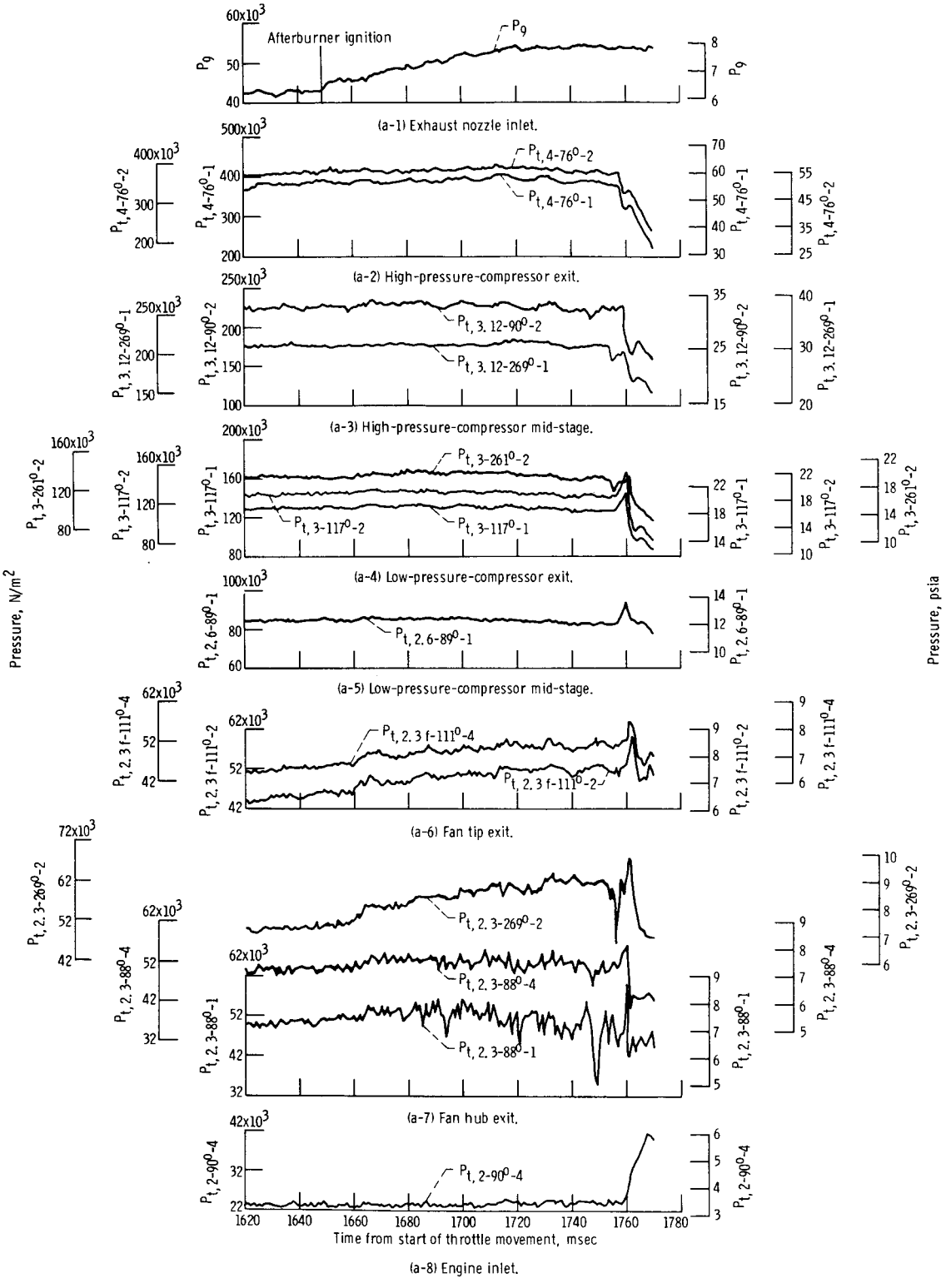

(a) Throttle burst from Military to Maximum throttle position.

Figure 10. - Typical variation of engine afterburning pressures during throttle movement, from Military to Maximum and Maximum to Military, during which stall occurred. Distortion-free engine-inlet flow. (Pressure probe locations are defined by axial station, circumferential angle and radial position, e.g., $P_{t,2-90^0-4}$. See fig. 1 for details.)

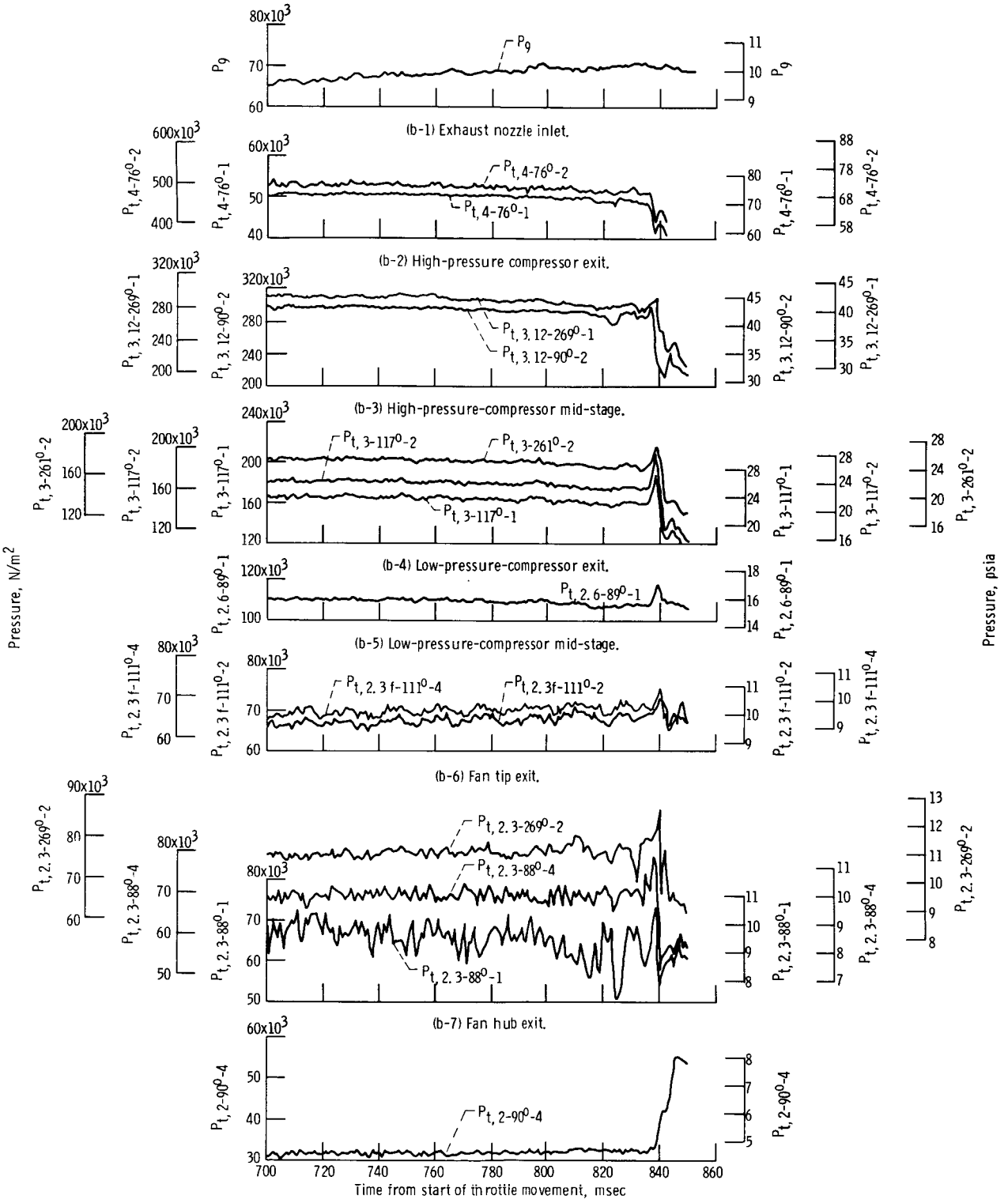

(b) Throttle chop from Maximum to Military throttle position.

Figure 10. - Concluded.

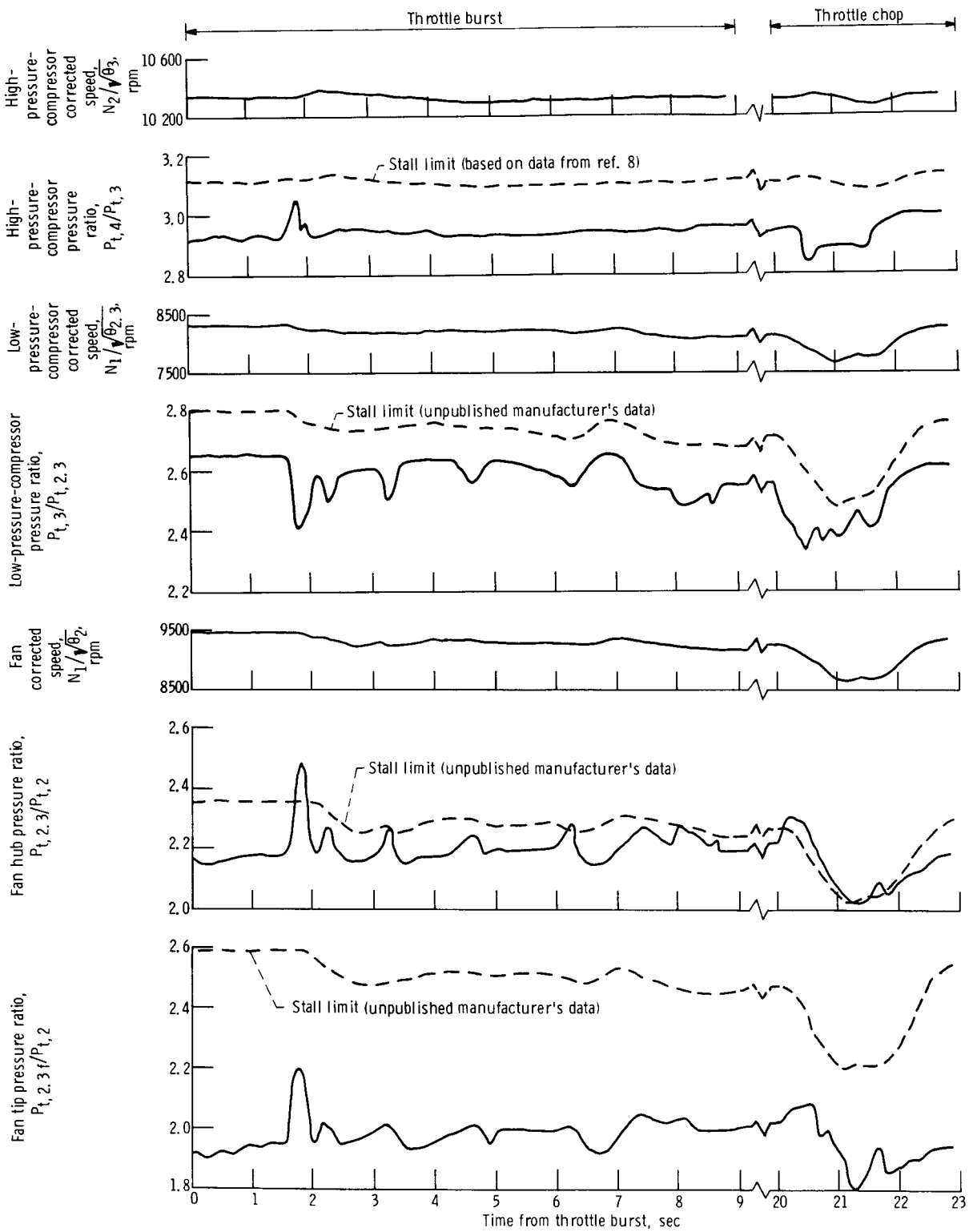

Figure 11. - Typical variation of operating points of fan tip and hub and low- and high-pressure compressors during stall-free throttle burst and chop between Military and Maximum throttle positions. Distortion-free engine-inlet flow.

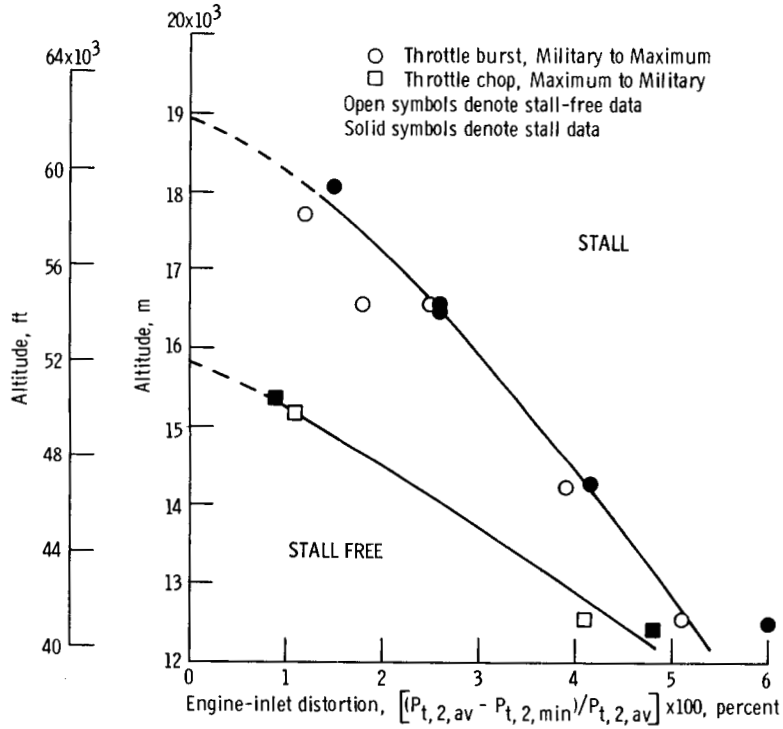

Figure 12. - Altitude-distortion limits during throttle transients, Military to Maximum and Maximum to Military. Air jet 180° distortion; simulated flight Mach number, 1.4; undistorted inlet recovery, 0.978; seventh- and 12th-stage bleeds closed.

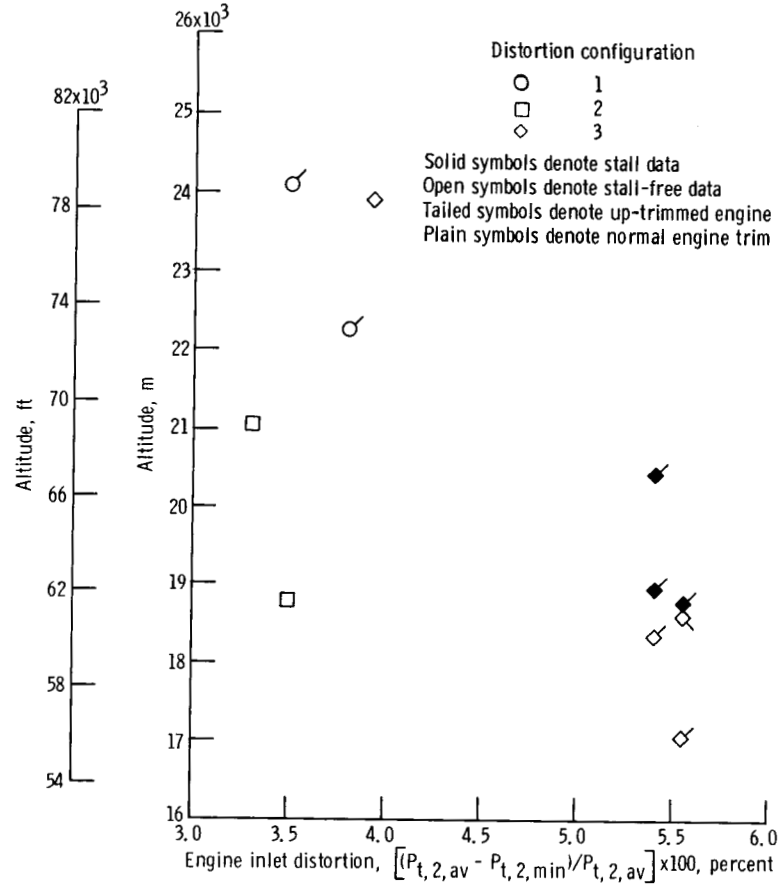

Figure 13. - Altitude distortion limits during throttle bursts, Military to Maximum. Screen distortion; simulated flight Mach number, 2.5; undistorted inlet recovery, 0.871; seventh-stage bleeds open; 12th-stage bleeds closed.

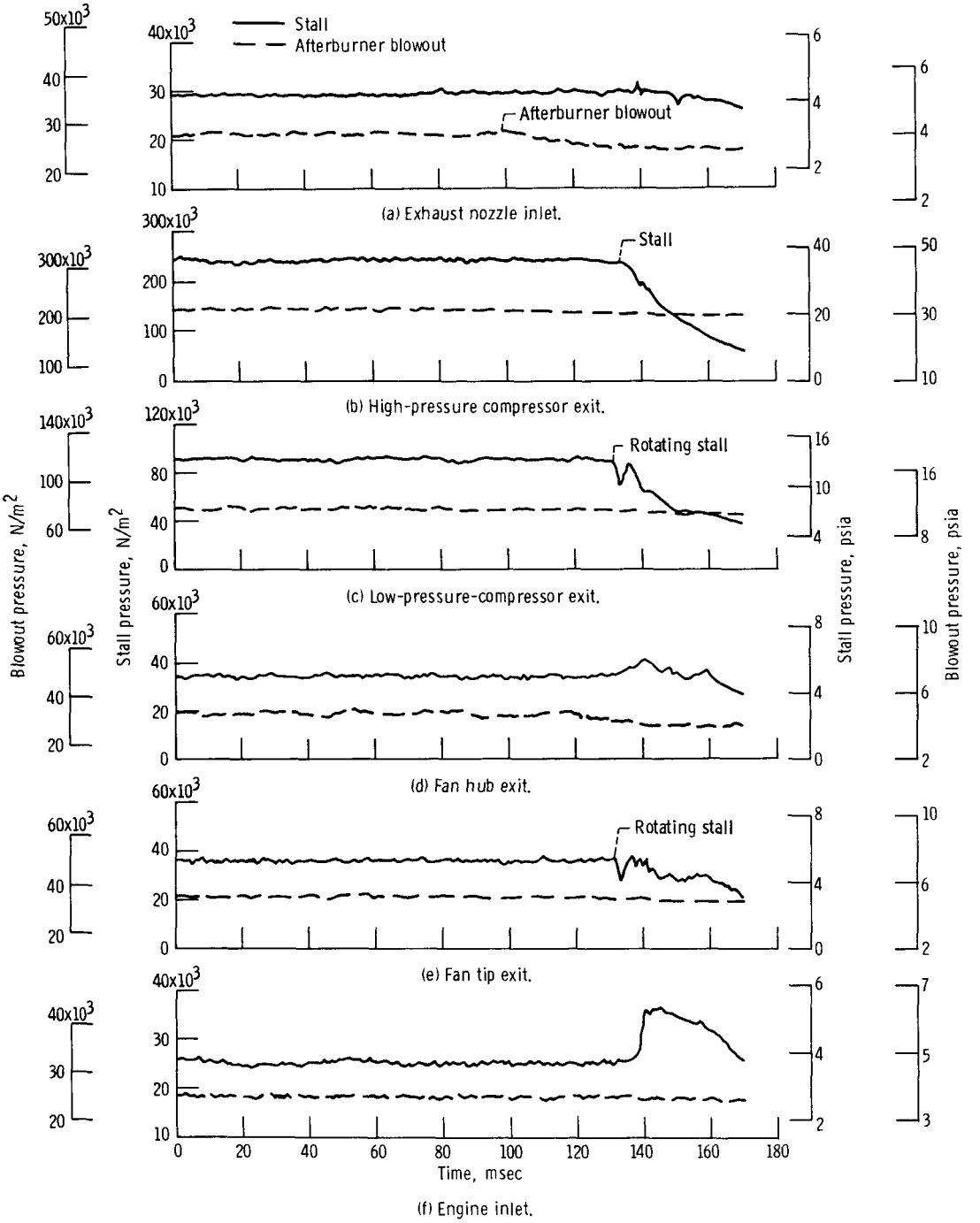

Figure 14. - Typical time history of engine afterburning parameters during stall and afterburning blowout with fixed throttle position. Distortion-free engine-inlet flow.

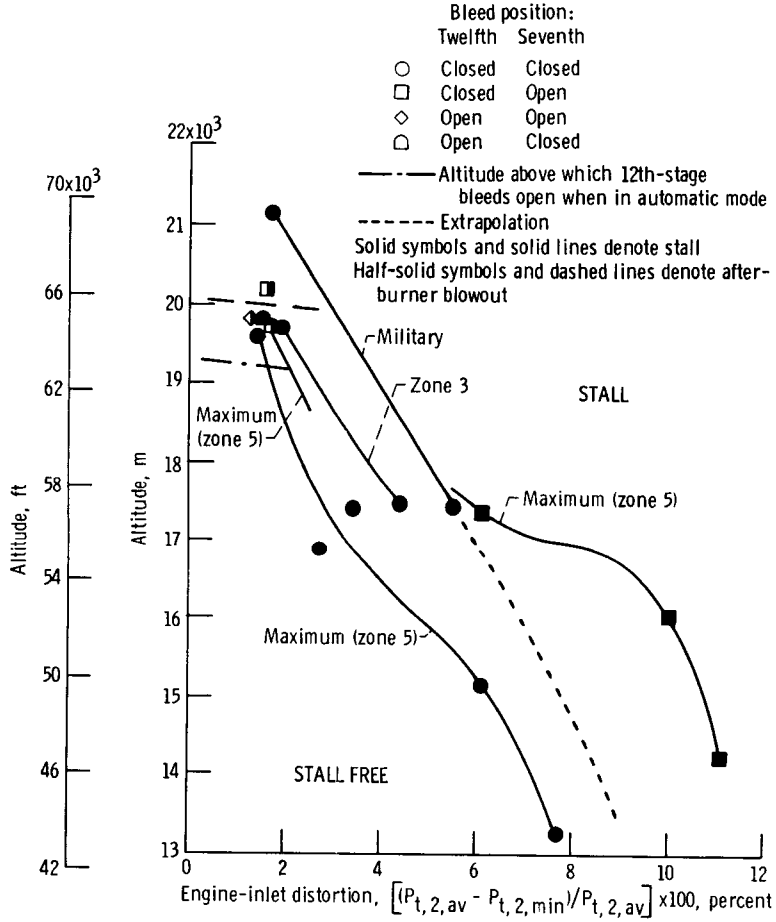

Figure 15. - Altitude-distortion limits at fixed throttle positions. Air jet 180° distortion; simulated flight Mach number, 1.4; undistorted inlet recovery, 0.978.

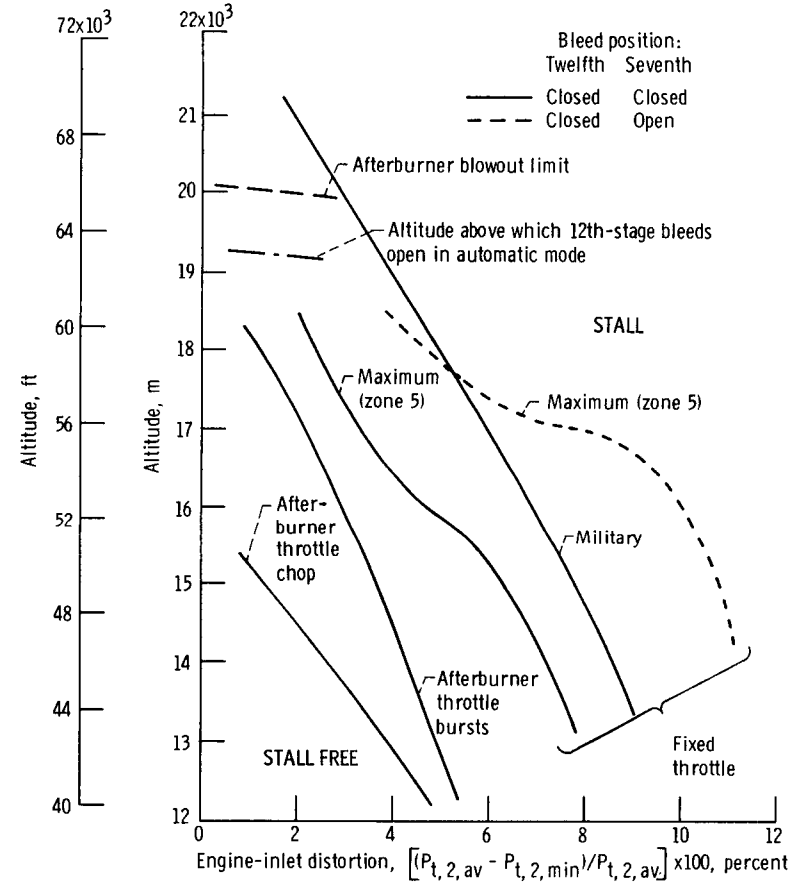

Figure 16. - Altitude-distortion limits. Air jet 180° distortion; simulated Mach number, 1.4; undistorted inlet recovery, 0.978.

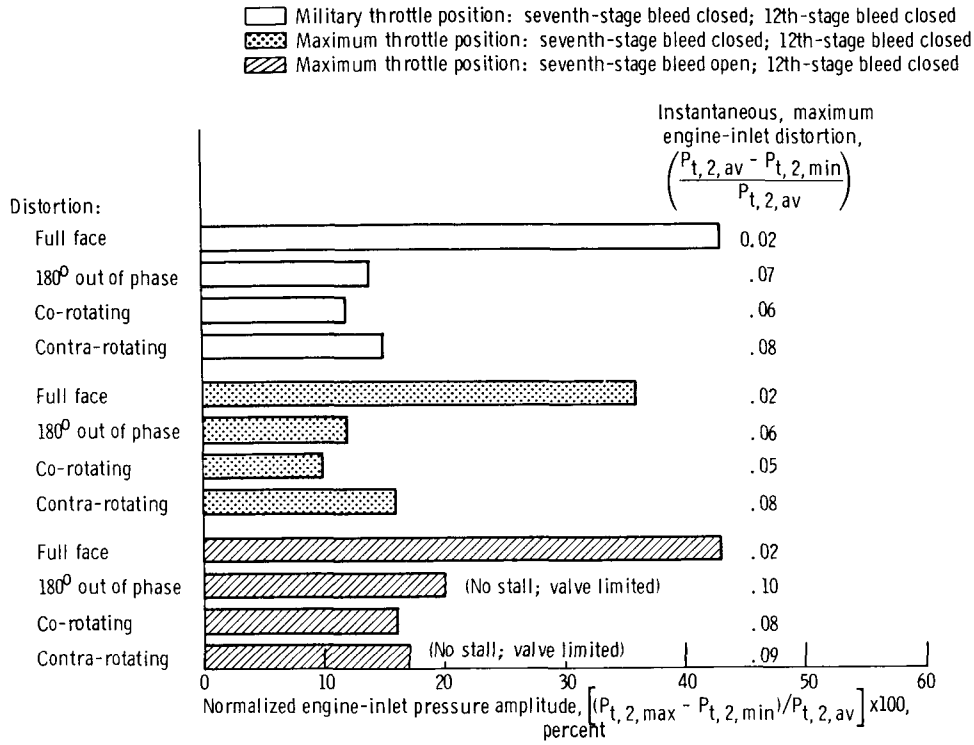

Figure 17. - Stall tolerance to dynamic engine-inlet pressure variations. Input frequency, 20 hertz; simulated flight Mach number, 1.4; altitude, 15 250 meters.

NASA-Langley, 1972 —— 2 E-6833

1. Report No. NASA TN D-6839	2. Government Accession No.	3. Recipient's Catalog No.
4. Title and Subtitle EXPERIMENTAL EVALUATION OF A TF30-P-3 TURBOFAN ENGINE IN AN ALTITUDE FACILITY: AFTERBURNER PERFORMANCE AND ENGINE-AFTERBURNER OPERATING LIMITS		5. Report Date July 1972 6. Performing Organization Code
7. Author(s) John E. McAulay and Mahmood Abdelwahab		8. Performing Organization Report No. E-6833 10. Work Unit No. 764-74 11. Contract or Grant No.
9. Performing Organization Name and Address Lewis Research Center, National Aeronautics and Space Administration, Cleveland, Ohio 44135		13. Type of Report and Period Covered Technical Note
12. Sponsoring Agency Name and Address National Aeronautics and Space Administration, Washington, D.C. 20546		14. Sponsoring Agency Code
15. Supplementary Notes		

16. Abstract

For distortion-free steady-state operation at the Maximum (full afterburning) throttle position, the afterburner combustion efficiency decreased from 0.91 to 0.68 as engine-inlet Reynolds number index was reduced from 0.80 to 0.25. Engine-afterburner operational limits were obtained for transient and fixed throttle operation over a range of engine-inlet distortions. At limiting conditions, time histories of pressures in the fan-compressor during throttle transients between Military and Maximum showed the development of rotating stall in the fan hub which quickly propagated and produced complete stall in the high-pressure compressor.

17. Key Words (Suggested by Author(s))	18. Distribution Statement
Turbofan Afterburner Compressor stall Inlet flow distortion	Unclassified - unlimited

19. Security Classif. (of this report)	20. Security Classif. (of this page)	21. No. of Pages	22. Price*
Unclassified	Unclassified	35	$3.00

* For sale by the National Technical Information Service, Springfield, Virginia 22151